

Combining Quinone-Based Cathode with an Efficient Borate Electrolyte for High-Performance Magnesium Batteries

Yanlei Xiu,^[a] Zhenyou Li,*^[a] Vinayan Bhaghavathi Parambath,^[a] Ziming Ding,^[b] Liping Wang,^[a] Adam Reupert,^[a] Maximilian Fichtner,^[a, b] and Zhirong Zhao-Karger*^[a]

Rechargeable magnesium batteries are gaining attention as promising candidates for large-scale energy storage applications because of their potentially high energy, safety and sustainability. However, the development of Mg batteries is impeded by the lack of efficient cathode materials and compatible electrode-electrolyte combinations. Herein, we demonstrate a new poly(1,4-anthraquinone)/Ketjenblack composite (14PAQ@KB) in combination with non-corrosive magne-

sium tetrakis(hexafluoroisopropoxy) borate $Mg[B(hfip)_4]_2$ ($hfip = OC(H)(CF_3)_2$) electrolyte towards high-energy and long-lifespan Mg batteries. This combination exhibits prominent electrochemical performance including a maximum discharge capacity of 242 mA h g^{-1} (approximately 93% of the theoretical capacity), superior cycling stability (81 mA h g^{-1} after 1000 cycles), and excellent rate capability (120 mA h g^{-1} at 5 C).

1. Introduction

Rechargeable magnesium batteries have emerged as a promising candidate for the next-generation battery technologies owing to their potentials of offering efficient, safe and sustainable energy storage solutions.^[1] However, the development of magnesium batteries is impeded by the lack of suitable cathode materials that enable reversible Mg-ion storage at a practically reasonable rate. Due to the high charge density of Mg-ion (120 C mm^{-3} of Mg^{2+} vs. 54 C mm^{-3} of Li^+), insertion of Mg-ions into the conventional inorganic oxide cathodes suffers from strong polarization and sluggish diffusion kinetics.^[2,3] Despite enormous efforts dedicated to the cathode development, very few of the proposed host structures practically outperformed the benchmark Chevrel Phase Mo_6S_8 reported more than 20 years ago,^[4] in terms of ion mobility and cyclability.

Organic cathodes have been considered as feasible alternatives to achieve high-energy, high-power Mg batteries.^[5–7] Compared to the dense inorganic crystal structures, organic materials generally have loosely packed structures bonded by

weak intermolecular forces, providing energetically more favorable ionic pathways. In particular, organic structures with certain degree of electron delocalization furtherly promote charge-redistribution, conducive to divalent Mg-ion storage and high-rate capability. Among them, quinone-based compounds based on thermodynamically favorable enolization reactions have attracted most of the attention so far.^[5] Due to the high solubility of both small molecule quinone derivatives and their magnesiated products,^[8] polymerization is usually applied as an improvement strategy to increase the reversible capacity and cycle life, and the ionic-liquid-based electrolytes also provide promising alternatives.^[9–11]

Taking into account the electrophilicity of the carbonyl groups, an non-nucleophilic electrolyte is a prerequisite for enabling reversible redox reactions of quinone-based polymers in Mg batteries.^[12] Additionally, the accessible capacity and capacity retention have been found to be strongly dependent on the electrolyte formulations. For instance, in $Mg(HMDS)_2\cdot 4MgCl_2/THF$ electrolyte, 1,4-polyanthraquinone (14PAQ) cathode provided a stable capacity of 79 mA h g^{-1} for 1000 cycles at 1 C (260 mA g^{-1}), after initial capacity drop from 110 mA h g^{-1} .^[13] A higher specific capacity of 165 mA h g^{-1} was achieved with a $Mg(TFSI)_2\cdot 2MgCl_2/DME$ electrolyte, but could not exceed 65% of its theoretical value (260 mA h g^{-1} , based on a two-electron reaction of each anthraquinone unit). A significant capacity reduction was observed once introducing $AlCl_3$ into the electrolyte, due to the detrimental interaction between the organic compound and the Al species.^[14] Moreover, the Mg-storage mechanism of 14PAQ notably differs depending on the electrolyte compositions. With the Cl-based electrolyte, an unique mechanism involving $MgCl^{+}$ shuttle instead of divalent Mg^{2+} ion as charge carrier was identified, leading to a reduced energy density at cell level.^[5,15] In addition, the corrosive nature of Cl-ions led to additional limitations in the operation of cells.^[16]

[a] Y. Xiu, Dr. Z. Li, Dr. V. Bhaghavathi Parambath, Dr. L. Wang, A. Reupert, Prof. M. Fichtner, Dr. Z. Zhao-Karger
Helmholtz Institute Ulm (HIU)
Helmholtzstr. 11, 89081 Ulm, Germany
E-mail: zhenyou.li@kit.edu
zhirong.zhao-karger@kit.edu

[b] Z. Ding, Prof. M. Fichtner
Institute of Nanotechnology (INT)
Karlsruhe Institute of Technology (KIT)
P.O. Box 3640, 76021 Karlsruhe, Germany.

 Supporting information for this article is available on the WWW under <https://doi.org/10.1002/batt.202100163>

 © 2021 The Authors. *Batteries & Supercaps* published by Wiley-VCH GmbH. This is an open access article under the terms of the Creative Commons Attribution License, which permits use, distribution and reproduction in any medium, provided the original work is properly cited.

Given the strong influence of electrolyte on the performance of the 14PAQ cathode, optimizing the electrolyte-electrode compatibility is crucial for achieving high-performance Mg batteries. Considering the vital role of Cl-free electrolyte in governing high-energy Mg battery systems and practical applicability, herein recently developed magnesium tetrakis (hexafluoroisopropoxy) borate $Mg[B(hfip)_4]_2$ ($hfip = OC(H)(CF_3)_2$) electrolyte^[17] was employed in the Mg-14PAQ system. The $Mg[B(hfip)_4]_2$ electrolyte (denoted as MBR) provides excellent electrolytic properties and is compatible with various Mg battery chemistries.^[18,19] Ketjenblack (denoted as KB) possesses a high specific surface area and prominent graphitic features,^[20] a cathode composite comprising 14PAQ and KB was prepared with incipient wet impregnation for a homogeneous distribution of the polymer, therefore enhanced electric conductivity and better access for the electrolyte. Electrochemical and mechanistic investigation with the abovementioned cathode-electrolyte combination exhibits a highly reversible, fast-kinetic and multi-electron redox reaction. Further optimization of the MBR electrolyte in terms of solvent and concentration leads to a less pronounced swelling of the polymer cathode, and hence an improved capacity retention. Further, the polymer-based Mg pouch cell is demonstrated and shows comprehensive implementation potentials. The current work provides general strategies to improve Mg-storage performance in polymer cathodes, aiming at high-capacity and long-lifespan Mg batteries.

2. Results and Discussion

2.1. Preparation and Structural Characterization of 14PAQ@KB

14PAQ was prepared according to the reported procedures.^[21] Details on preparation and characterization are provided in the Supporting Information. As shown in Figure S1, the 1H NMR spectrum exhibits multiple peaks (7.74–8.34 ppm) referring to the aromatic hydrogens in the anthraquinone moieties. A signal at 1671 cm^{-1} in the FT-IR spectrum corresponds to the characteristic bands of the stretching vibrations of carbonyl groups (Figure S2). To improve the electronic conductivity of the polymer, the synthesized 14PAQ was well incorporated with the high-surface-area conductive carbon matrix Ketjenblack EC-600JD (KB) ($S_{BET} = 1270\text{ m}^2\text{ g}^{-1}$)^[20] via a solution impregnation approach as shown in Figure 1(a). Briefly, 14PAQ was dissolved in chloroform ($CHCl_3$), and then KB was added to the solution with a mass ratio of 1:1. The suspension was stirred and ultrasonicated to ensure a highly dispersion of the polymer on the surface of the carbon. After removal of the solvent, the composite was dried in vacuum at 60°C overnight. The morphological structures of the pristine KB and 14PAQ@KB composite were characterized by SEM and TEM. As shown in Figure 1(b–d), the pristine KB appears as 30–100 nm long aggregates consisting of hollow carbon spheres. After loading, the primary KB aggregates were covered with the 14PAQ and connected as composite clusters (Figure 1e, f). The high-resolution transition electron microscope (HRTEM) images reveal that the composite particles exhibit the graphitic walls of the hollow KB particles, while the amorphous area suggests the polymer film on the carbon surface (Figure 1g).

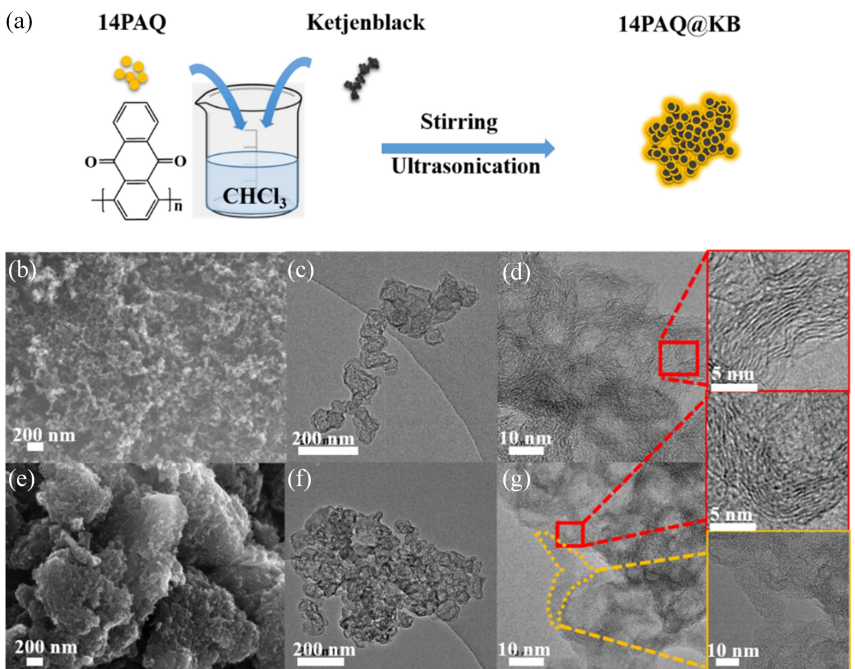


Figure 1. (a) Schematic illustration of 14PAQ@KB composite preparation; SEM and HRTEM images of (b–d) pristine Ketjenblack and (e–g) 14PAQ@KB composite.

2.2. Electrochemical Performance of 14PAQ@KB Cathode with Mg[B(hfip)₄]₂ Electrolytes

Electrochemical properties of the 14PAQ@KB cathode in the new Cl-free borate electrolyte were firstly investigated by cyclic voltammetry (CV) in a three-electrode PAT-Cell (EL-CELL) using the 14PAQ@KB as the working electrode (WE), polished Mg foils as both the counter and reference electrode (Mg_{CE} and Mg_{RE}) with 0.3 M Mg[B(hfip)₄]₂/DME (also denoted as MBR/G1) electrolytes. As shown in Figure 2(a), one broad reduction peak existed at 1.19 V during the first anodic scan, while a main oxidation peak was found at 1.75 V in the reverse scan, which corresponded to the reversible enolization reactions of 14PAQ. In the following scan cycles, the reduction peak shifted to ~1.40 V and a similar shift appeared in the CV profiles of WE vs. Mg_{CE} (Figure S3a), indicating an activation process at the cathode. As a result, the potential difference between the reduction and oxidation peaks decreased to 0.26 V, and it remained constant in the extended cycles, implying the high

redox reversibility of 14PAQ in the borate electrolytes. The small shoulder peaks in the CV curves could be ascribed to the stepwise reactions with different accessibility of Mg-ions to the carbonyl groups of the polymer matrix.

The electrochemical performance of the 14PAQ@KB cathode in MBR electrolytes was evaluated with coin cells in a voltage window between 0.5 and 2.5 V. Initially, 0.3 M MBR/G1 electrolyte was employed for the Mg-14PAQ@KB cells; however, an unsatisfied capacity retention was observed in the cycling stability tests, where the discharge capacity dropped from the initial 240 to 78 mA h g⁻¹ after 500 cycles (Figure S3b). To clarify this issue, post-mortem analysis of the cycled cathodes was carried out by SEM. It was found that the dense and smooth surface of the as-prepared cathode became coarse and loose after cycling (Figure S3c, d). The drastic morphological change of the cathodes could be caused by polymer swelling after soaking in the electrolyte, which weakened the mechanical integrity of the cathode structure. To mitigate the swelling behavior, the concentration of the MBR/G1 electrolyte was

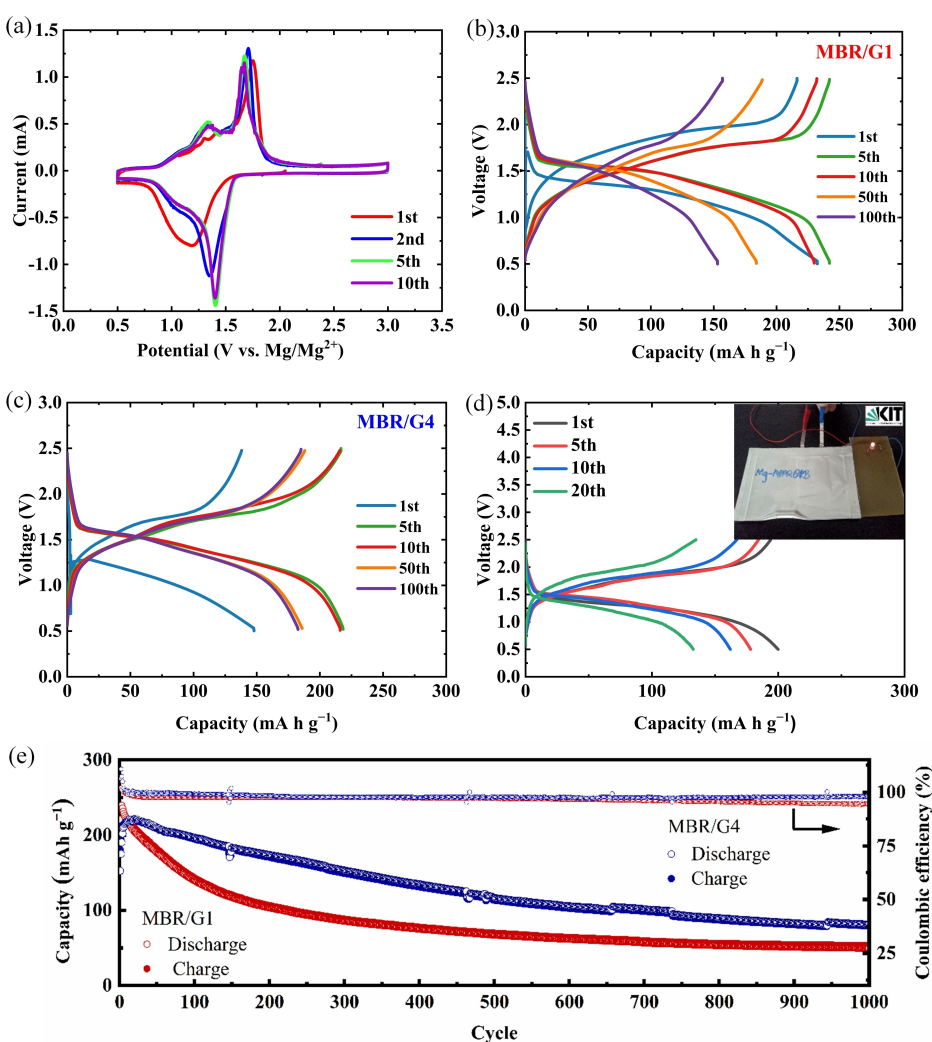


Figure 2. (a) CV curves of the 14PAQ@KB cathode vs. Mg_{RE} at a scan rate of 0.5 mVs⁻¹ with 0.3 M MBR/G1 electrolyte, Galvanostatic voltage profiles of the composite cathode at 1 C with 0.5 M electrolyte of (b) MBR/G1, (c) MBR/G4. (d) Electrochemical performance of the Mg-14PAQ@KB pouch cell with 0.5 M MBR/G4 at 0.1 C and the inset shows the photograph of the lab pouch cell. (e) Cycling performance of the 14PAQ@KB cathode with MBR/G1 and MBR/G4 electrolytes at 1 C.

increased to its solubility limit (~ 0.5 M) and the viscous long-chain tetraglyme (G4) was further used to prepare a saturated MBR/G4 electrolyte (~ 0.5 M). The reversibly Mg plating-stripping and rate performance of the 0.5 M MBR/G4 electrolyte were examined with symmetric Mg|Mg cells, which exhibited a low voltage polarization (< 0.2 V at 0.3 mA cm^{-2} , up to 300 h) as presented in Figure S4. As shown in Figure 2(b), the voltage profile for 14PAQ@KB in 0.5 M MBR/G1 electrolytes at 1 C (260 mA g^{-1}) exhibits one discharge plateau with an average voltage of 1.25 V and an initial discharge capacity 220 mA g^{-1} , corresponding to two-electron reduction of the 14PAQ monomer units. After 5 cycles, the discharge capacity reached to 242 mA g^{-1} , which is almost 93% of the theoretical capacity (260 mA g^{-1}). To the best of our knowledge, this is the highest capacity for polyanthraquinone (PAQ)-based cathode materials in Mg batteries so far. Moreover, the average discharge potential increased to 1.48 V, resulting in a minor voltage hysteresis, which agreed with the shift of the reductive peaks and enhanced current observed in the CV cycling. This activation process could be related to the native oxide and the adlayer of the electrolyte components on the Mg anode, which may impede the charge transfer at electrolyte-anode interface. Upon cycling, freshly formed active Mg deposits on the anode surface can improve the interfacial kinetics. The interface conditioning process of the borate electrolytes has also been investigated in other separated studies with Mg–Mg symmetric cells.^[18,19]

The Mg-14PAQ@KB cells with 0.5 M MBR/G4 behaved similarly as those with MBR/G1 electrolytes, displaying gradually increased capacity and slightly reduced overpotential

during the first cycles (Figure 2c). Notably, in the cyclability tests, the cells with 0.5 M MBR/G4 electrolyte maintained a capacity of 116 mA g^{-1} after 500 cycles and 81 mA g^{-1} after 1000 cycles, while the cells with 0.5 M MBR/G1 electrolyte delivered an inferior capacity of 50 mA g^{-1} after 1000 cycles (Figure 2e). At a higher c-rate (2 C), the cell with 0.5 M MBR/G4 electrolyte could be cycled for 2000 cycles with a capacity retention of 50 mA g^{-1} (Figure S5a). As a proof of concept, a lab pouch cell was assembled with the 14PAQ@KB cathode at a mass loading of 2.5 mg cm^{-2} and 0.5 M MBR/G4 electrolyte (Figure S5b). As shown in Figure 2(d), the cell delivered a specific capacity of 202 mA g^{-1} at 0.1 C. Note that the conductive carbon (KB) has a negligible capacity contribution in the 14PAQ@KB electrode (Figure S6).

Further, the rate capability was evaluated, in which Mg-14PAQ@KB cells with MBR/G1 electrolyte exhibited a better capacity retention at higher current rates (Figure 3a–c). For instance, a capacity of 120 mA g^{-1} was obtained at 5 C, corresponding to a power density of 885 W kg^{-1} , which surpassed the previously reported 14PAQ combined with other types of Mg-electrolytes (Figure 3d). Besides, the energy density of 373.5 Wh kg^{-1} (obtained from the maximal specific capacity) was also superior to the benchmarking inorganic intercalation-type cathode materials for RMBs (105 Wh kg^{-1} for Mo_6S_8 ^[4] and 123 Wh kg^{-1} for Ti_2S_4 ^[22]). The cell with 0.5 M MBR/G4 electrolyte exhibited more stable Coulombic efficiency (CE) at different currents, while a relatively low CE value was observed for the cell with 0.5 M MBR/G1 electrolyte cycling at a lower C-rate i.e., 0.5 C (Figure S7).

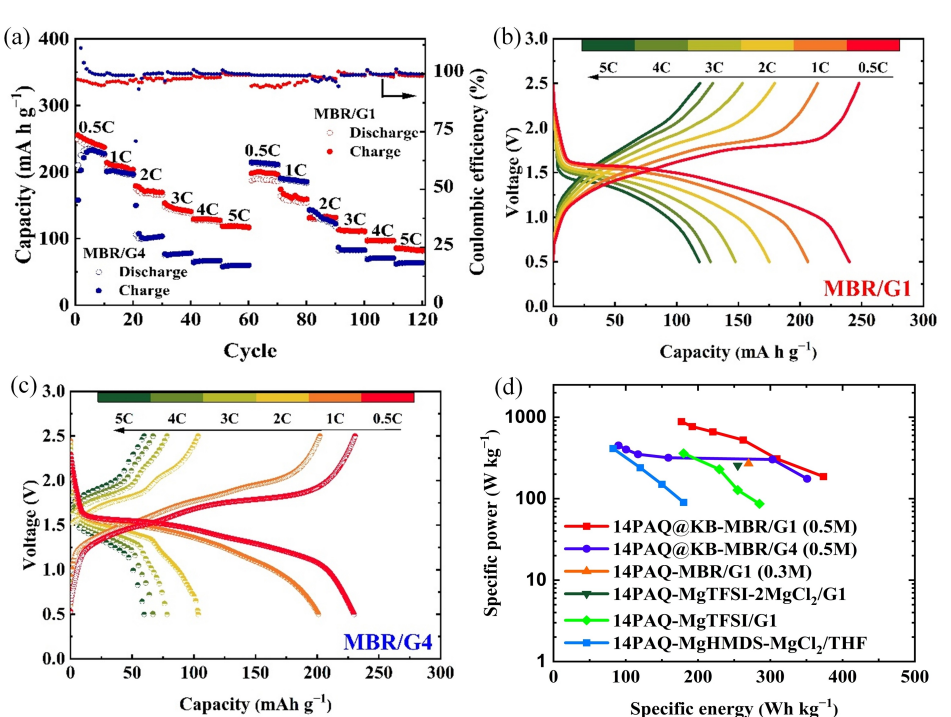


Figure 3. (a) Rate capability of the 14PAQ@KB cathode with MBR/G1 and MBR/G4 electrolytes, respectively. Corresponding galvanostatic voltage profiles of the 5th cycle at each C-rate (0.5 to 5 C, 1 C refers to 260 mA g^{-1} , 5th cycle of each c-rate test in the first sequence); (b) MBR/G1, (c) MBR/G4. (d) Ragone plots showing the performance of 14PAQ-based cathodes with different Mg electrolytes.

Besides the positive impacts of employed MBR-based electrolyte on the battery performance, the higher accessible capacity in this work might also have benefited from the solution impregnation method, which ensured a homogeneous dispersion of 14PAQ on the high-surface conductive carbon, hence offering improved electric conductivity and accessibility of the electrolyte to the redox-active moieties in the cathode. As shown in Figure S8, the 14PAQ-KB electrode prepared with mechanical milling only yielded the highest capacity of 175 mAh g^{-1} with 0.3 M MBR/G1 electrolyte, and 80 mAh g^{-1} was maintained after 100 cycles.

It needs to be mentioned that a formation process (sharp voltage dip and negligible capacity) was observed with both cell setups with saturated MBR/G1 and MBR/G4 electrolyte, respectively (Figure S9). To understand the origin of this formation behavior, three-electrode PAT-Cells were constructed consisting of the 14PAQ@KB cathode as WE, Mg foils as CE and RE, respectively. A galvanostatic measurement was conducted in a voltage range of 0.5–2.5 V vs. Mg_{CE} . Figure 4(a) shows the voltage profiles of WE-RE, WE-CE and CE-RE during the typical formation cycles, respectively. A large overpotential ($\sim 1.3 \text{ V}$) between the Mg_{CE} and RE was observed, indicating the large polarization on the Mg anode.

The large overpotentials of Mg anode could be linked to the high anode impedance, which exceeded $500 \text{ k}\Omega \text{ cm}^2$ after 20 h resting [Figure 4(b)]. Compared to the cathode impedance [$0.9 \text{ k}\Omega \text{ cm}^2$, Figure 4(c)], anode impedance was dominant and limited the charge transfer of the cell operation [Figure 4(d)].

This unique anode-electrolyte interfacial phenomenon under static condition was believed to be originated from the electrochemically inactive species adsorbed on the Mg surface.^[18,23] When operating the cell, the adsorption layer was disturbed by the bias voltage and the polarization at the anode gradually alleviated. After the formation cycles, the impedance was reduced significantly to approximately $0.2 \text{ k}\Omega \text{ cm}^2$ after the 10th cycle.

2.3. Charge Storage Mechanisms of 14PAQ@KB Cathode

The Mg-storage mechanism of 14PAQ was studied by means of operando Raman spectroscopy. The Raman spectra of the cathode were recorded at different discharge/charge states in the first cycle, as shown in Figure 5. The D/G bands of KB, which locate at $\sim 1323 \text{ cm}^{-1}$ and 1600 cm^{-1} as shown in Figure S10 overlap with the stretching vibration of the carbonyl moiety in 14PAQ at 1660 cm^{-1} (Figure S11). Nevertheless, the evolution of the Raman shifts could be visualized by probing the changes of the enolate group (the redox-active group at a reduction state, see Figure 5a) and its neighboring moieties. During discharging process, the Raman shift at 1295 cm^{-1} assigned to the stretching vibration of the enolate moiety $\text{C}-\text{O}^-$ ^[24] appeared and the intensity gradually increased, while the intensity decreasing of the Raman bands was observed at 1590 cm^{-1} and $1600-1660 \text{ cm}^{-1}$ corresponding to the stretching mode of $\text{C}=\text{C}$ and $\text{C}=\text{O}$ bonds, respectively.^[25] This indicates

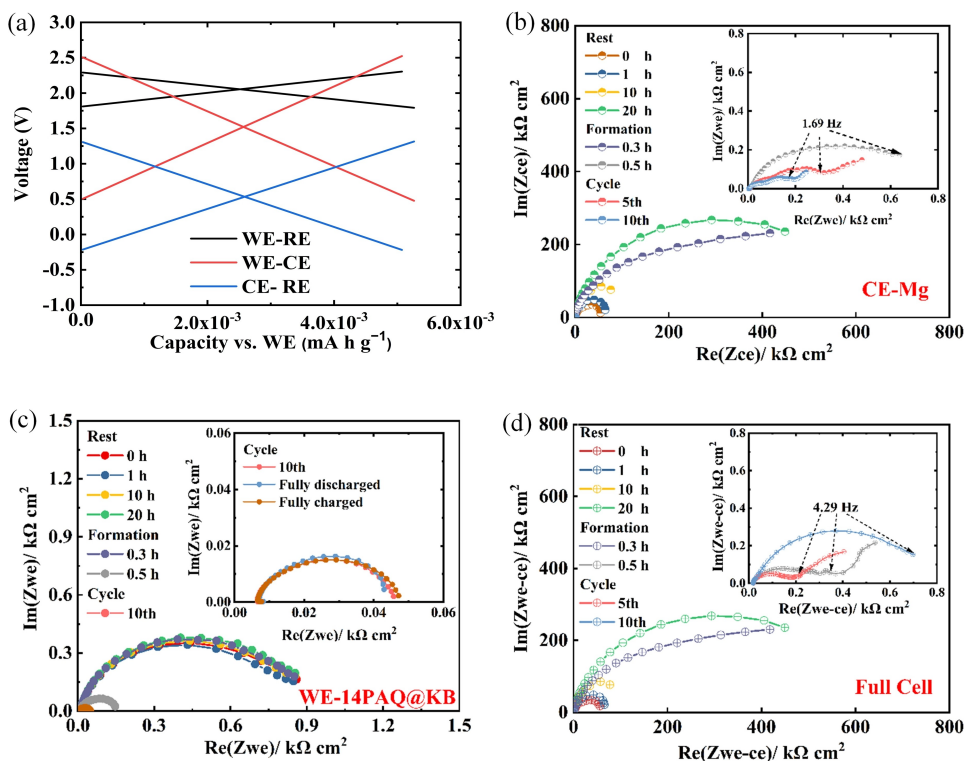


Figure 4. Mg-14PAQ@KB cells with 0.5 M MBR/G4 electrolyte: (a) Galvanostatic discharge/charge profile of three-electrode configuration at 1 C: counter electrode (CE), working electrode (WE), and full cell (WE-CE), capacity normalized by the weight of working electrode. Nyquist plots of three-electrode configuration: (b) anode, (c) cathode, (d) full cell.

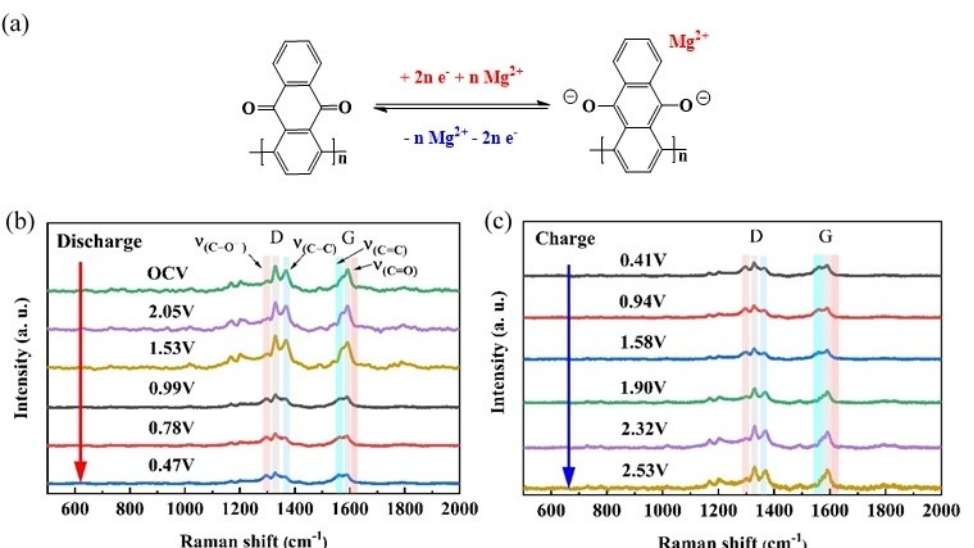


Figure 5. (a) Schematic diagram of the stepwise two-electron redox mechanism for 14PAQ. Operando Raman spectra of 14PAQ@KB cathode in different electrochemical states in the first cycle: (b) discharge and (c) charge.

that the C=O bonds have transformed to C–O[−] groups in the magnesiation process, and the intensity of the peak at 1365 cm^{−1} corresponding to the stretching mode of the C–C bonds^[26] in the phenyl rings decreased, simultaneously, which implies an electron redistribution within the conjugated structure during the enolization reaction. After charging (Figure 5c), the Raman spectra was almost restored as its initial state, which confirms the reversible Mg-storage mechanism of 14PAQ in the borate electrolyte. It should be noticed that the Raman signals in the range of 710–863 cm^{−1} indicating the stretching vibration of CF₃ groups in the [B(hfip)₄][−] anion of the MBR electrolyte (Figure S11)^[27] were not detected during the discharge process, manifesting no anion co-inserted into the 14PAQ cathode in this cell configuration.

2.4. Kinetic Investigation of 14PAQ@KB Cathode

To study the reaction kinetics of 14PAQ@KB cathode, CV measurements at different scan rates were carried out as shown in Figure 6(a). The relation of scan rates and current response was analyzed by an empirical Randles-Sevcik equation [Eq. (1)]:

$$i = av^b \quad (1)$$

where, i , a , and b are the peak current and the adjustable parameters to scan rate v , respectively. The fitted b -values of both reduction and oxidation were higher than 0.85 (Figure 6b) and indicated the obvious fast surface-control-dominant processes.^[28]

The diffusion coefficient of Mg²⁺ ions in 14PAQ@KB cathode was further determined by the galvanostatic intermittent titration technique (GITT). Based on the GITT profile carried out at the 10th cycle (Figures 6c, S12), the diffusion coefficient

D^{GITT} of the discharge process was calculated according to Equation (2):

$$D^{\text{GITT}} = \frac{4}{\pi\tau} \left(\frac{m_B V_m}{M_B S} \right)^2 \left(\frac{\Delta E_s}{\Delta E_t} \right)^2 \quad (2)$$

where, τ , m_B , V_m , M_B , S , ΔE_s , and ΔE_t are the constant current pulse time, the mass of cathode material, molar mass, molar volume (194.72 cm³ mol^{−1}, calculated as shown in Supporting Information), interface area of electrode/electrolyte (the geometric area of the cathode, 0.78 cm²), the voltage changes of each step (relaxation, included) and difference of cell voltage in constant current (IR-drop excluded), respectively.^[29] The results shown in Figure 6d imply that the Mg²⁺ diffusivity persisted at around $(8.19 \pm 4.56) \times 10^{-10}$ cm² s^{−1} in the main redox region (< 1.6 V). Besides, the diffusion coefficient was also deduced by using the CVs and the resultant values were all in a magnitude of 10^{−9} cm² s^{−1} (Table S1), which agreed with the result from GITT. These values were notably higher than some typical inorganic intercalation cathodes and also organic compounds for Mg storage (diffusion coefficients of Mg²⁺ for Mo₆S₈,^[30] TiS₂, VS₂, TiSe₂, VSe₂,^[31] and PI@CNT^[32] are $\sim 9 \times 10^{-12}$, 3.10×10^{-22} , 3.20×10^{-22} , 4.85×10^{-19} , 6.73×10^{-19} , 4.48×10^{-12} cm² s^{−1}, respectively). The fast diffusion kinetics of Mg²⁺ in the 14PAQ@KB composite might originate from the solution impregnation processing and the fast surface-control-dominant processes. The unique structure with the thin layer of the polymer constructed on the porous carbon matrix may have provided a beneficial electrolyte-polymer interface, shortened the diffusion pathways, and consequently facilitating electron transfer and Mg-ion mobility.^[33]

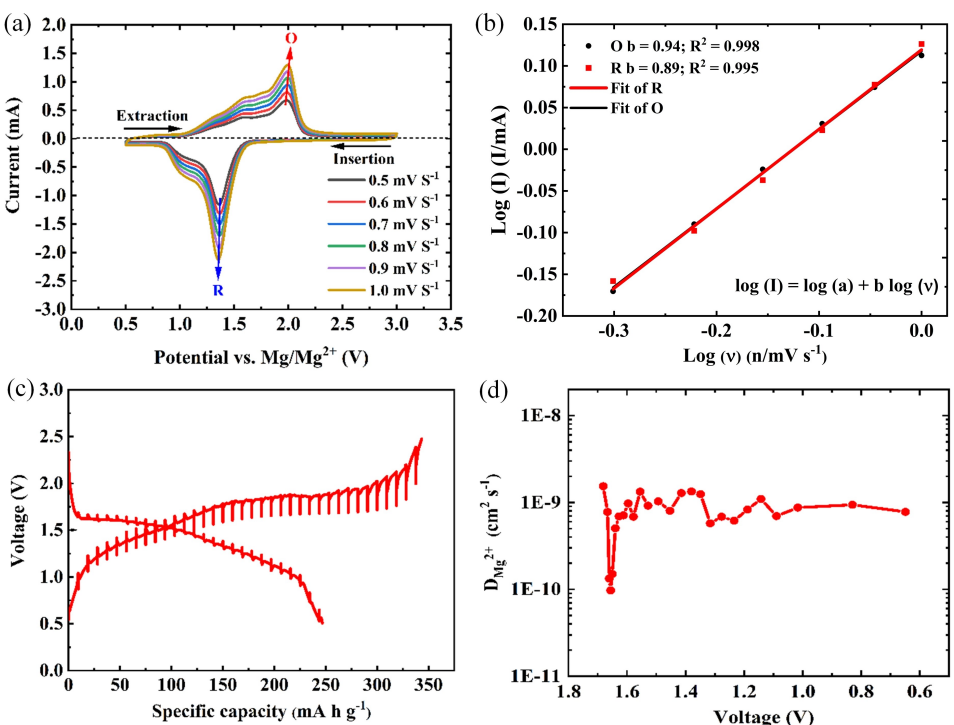


Figure 6. (a) CVs at various scan rates from 0.5 to 1 mV s^{-1} , (b) current response versus scan rate ($\log I$ vs. $\log v$) plotted at the main redox peaks. (c) GITT curve of Mg-14PAQ@KB cell at the 10th cycle, (d) diffusivity of Mg-ions determined from the GITT measurement during the discharge process.

3. Conclusions

In summary, 14PAQ@KB composite as a polymer cathode material was fabricated by a solution dispersion method. The incorporation of the polymer film on the surface of the carbon structure could provide sufficient effective cathode-electrolyte interfaces and facilitate the charge and ion transfer during the electrochemical processes. As a result, fast Mg^{2+} ion mobility and redox kinetics were enabled by the shortened solid diffusion pathways. The 14PAQ@KB cathodes in combination with a Cl-free $\text{Mg}[\text{B}(\text{hfip})_4]_2$ electrolyte exhibited superior electrochemical performance in terms of rate capability, high-power, high-energy density and long-term cycling stability. By employing high-viscous $\text{Mg}[\text{B}(\text{hfip})_4]_2$ /tetraglyme electrolytes, the 14PAQ@KB cathodes could be cycled for at least 1000 cycles with a capacity retention of 81 mA h g^{-1} . Furthermore, the prototype Mg-14PAQ@KB pouch cell has been validated. The polymer composite fabrication method and cathode-electrolyte combination strategies could be implemented to other cathodes towards long-lifespan, fast-kinetic Mg batteries.

Experimental Section

Materials preparation

The electrolyte salt of magnesium tetrakis(hexafluoroisopropoxy)borate (MBR) was synthesized following our previous report.^[17] 14PAQ was prepared according to the literature.^[21] The detailed synthetic procedures can be found in the Supporting Information. The as synthesized 14PAQ was dissolved in chloroform and mixed

with Ketjenblack EC600JD (KB) in a mass ratio of 1:1. After vigorously stirring under argon for 24 h, the suspension was placed in an ultrasonic bath for 2 h. To obtain the final 14PAQ@KB composite, the mixture was dried under vacuum before ball-milling at 200 rpm for 2 h.

Characterizations

The 14PAQ was characterized through nuclear magnetic resonance spectroscopy (NMR, Bruker Advance II 500 spectrometer) using CDCl_3 as solvents and Fourier-transform infrared spectroscopy (FT-IR, Spectrum Two, PERKIN ELMER). The morphology of Ketjenblack, 14PAQ@KB composite, and the electrodes were characterized by SEM (ZEISS LEO 1530, at 15 kV) and TEM (Philips Tecnai F20, at 200 kV).

Operando Raman spectroscopy was utilized to analyze the 14PAQ@KB cathode during the discharge and charge processes. The spectra were collected at room temperature in the spectral range 500–2000 cm^{-1} by using inVia™ confocal Raman microscope (RENISHAW) with a 633 nm excitation laser. The nominal laser power was filtered down to ~2.5 mW to avoid over sample heating. The slit opening of the confocal system was fixed at 65 μm and centered at 1867 μm . The spectra were collected in backscattering geometry with a 50X objective (confocal micro-Raman mode). To increase the signal-to-noise ratio, each spectrum is the average of 5 accumulations with 5 s each. The probed sample spot was continuously focused during the experiment using an autofocus function. The Raman data were analyzed using inVia WiRE 4.4 Software. Operando Raman measurements were conducted using an ECC-Opto-Std (EL-CELL® GmbH) electrochemical cell connected with Raman microscope. The 14PAQ@KB composite used for operando Raman measurement was prepared by following the abovementioned procedure with a 14PAQ: KB ratio of 9: 1 (w/w). The in-situ cell was assembled using the

14PAQ@KB composite as a positive electrode, Mg metal as an anode. The cathode side of the cell was sealed with a thin optical glass window (0.15 mm) and made air-tight with a rubber seal. The battery tester was an Interface 1000TM Potentiostat/Galvanostat/ZRA (Gamry Instruments, Inc.) electrochemical workstation with "Gamry Echem Analyst" software.

Electrochemical measurements

The cathode was prepared by mixing the 14PAQ@KB composite with polytetrafluoroethylene (PTFE) binder in ethanol at a mass ratio of 9:1 and dried at 85 °C for 12 h under vacuum. The mixture was then pressed onto an aluminum mesh with a mass loading of 1 to 1.5 mg cm⁻² in an argon-filled glove box ($H_2O, O_2 < 0.1$ ppm). All electrochemical measurements were conducted with coin cells (CR2032), except for the three-electrode cyclic voltammetry (CV) and impedance measurements using a PAT-Cell configuration (EL-Cell). Each tested coin cell was comprised of a polished Mg-foil anode, a 14PAQ@KB cathode, one Celgard 2340, and one Whatman GF/C separator. 0.3 M MBR/DME (MBR/G1) solution was used as the electrolyte unless otherwise indicated. CV tests were carried out using the VMP3 potentiostat (Bio-Logic), while galvanostatic cycling and GITT measurements were conducted with an Arbin battery tester at 25 °C. The 14PAQ@KB cathode for pouch cell was prepared by following the abovementioned procedure, specifically, in the size of 3×4 cm with an active mass loading of 2.5 mg cm⁻² (14PAQ) and dried at 80 °C for 12 h under vacuum. The pouch cell was assembled with the same configuration of coin cell in a dry room and 0.5 M MBR/G4 was used as the electrolyte.

Supporting Information

Supporting Information is available from the Wiley Online Library or from the author.

Acknowledgements

We would like to acknowledge the European Union's Horizon 2020 research and innovation program under grant agreement No 824066 via the "E-MAGIC" project. This work contributes to the research performed at CELEST (Center for Electrochemical Energy Storage Ulm-Karlsruhe) and was partly funded by the German Research Foundation (DFG) under Project ID 390874152 (POLiS Cluster of Excellence). The authors acknowledge the support from the Karlsruhe Nano Facility (KNMF) for electron microscopy and spectroscopy. Open Access funding enabled and organized by Projekt DEAL.

Conflict of Interest

The authors declare no conflict of interest.

Keywords: borate · chlorine-free electrolyte · magnesium battery · organic cathode material · quinone-based cathode

- [1] R. Mohtadi, O. Tutusaus, T. S. Arthur, Z. Zhao-Karger, M. Fichtner, *Joule* **2021**, *5*, 581.
- [2] S. Tepavcevic, Y. Liu, D. Zhou, B. Lai, J. Maser, X. Zuo, H. Chan, P. Král, C. S. Johnson, V. Stamenkovic, N. M. Markovic, T. Rajh, *ACS Nano* **2015**, *9*, 8194.
- [3] J. S. Kim, W. S. Chang, R. H. Kim, D. Y. Kim, D. W. Han, K. H. Lee, S. S. Lee, S. G. Doo, *J. Power Sources* **2015**, *273*, 210.
- [4] D. Aurbach, Z. Lu, A. Schechter, Y. Gofer, H. Gizbar, R. Turgeman, Y. Cohen, M. Moshkovich, E. Levi, *Nature* **2000**, *407*, 13.
- [5] Z. Zhao-Karger, M. Fichtner, *Front. Chem.* **2019**, *7*, 1.
- [6] H. Dong, Y. Liang, O. Tutusaus, R. Mohtadi, Y. Zhang, F. Hao, Y. Yao, *Joule* **2019**, *3*, 782.
- [7] H. Dong, O. Tutusaus, Y. Liang, Y. Zhang, Z. Lebens-Higgins, W. Yang, R. Mohtadi, Y. Yao, *Nat. Energy* **2020**, *5*, 1043.
- [8] B. Pan, D. Zhou, J. Huang, L. Zhang, A. K. Burrell, J. T. Vaughey, Z. Zhang, C. Liao, *J. Electrochem. Soc.* **2016**, *163*, A580.
- [9] J. Xie, Q. Zhang, *Small* **2019**, *15*, 1.
- [10] J. Bitenc, T. Pavčnik, U. Košir, K. Pirnat, *Materials* **2020**, *13*, 506.
- [11] W. Zhou, M. Zhang, X. Kong, W. Huang, Q. Zhang, *Adv. Sci.* **2021**, *8*, 2004490.
- [12] J. Bitenc, K. Pirnat, T. Bančič, M. Gaberšček, B. Genorio, A. Randon-Vitanova, R. Dominko, *ChemSusChem* **2015**, *8*, 4128.
- [13] B. Pan, J. Huang, Z. Feng, L. Zeng, M. He, L. Zhang, J. T. Vaughey, M. J. Bedzyk, P. Fenter, Z. Zhang, A. K. Burrell, C. Liao, *Adv. Energy Mater.* **2016**, *6*, 2.
- [14] J. Bitenc, K. Pirnat, E. Žagar, A. Randon-Vitanova, R. Dominko, *J. Power Sources* **2019**, *430*, 90.
- [15] T. Pavčnik, J. Bitenc, K. Pirnat, R. Dominko, *Batteries & Supercaps* **2021**, *4*, 815.
- [16] C. Wall, Z. K. Zhirong, M. Fichtner, *ECS Electrochem. Lett.* **2015**, *4*, C8.
- [17] Z. Zhao-Karger, M. E. Gil Bardaji, O. Fuhr, M. Fichtner, *J. Mater. Chem. A* **2017**, *5*, 10815.
- [18] Z. Zhao-Karger, R. Liu, W. Dai, Z. Li, T. Diemant, B. P. Vinayan, C. Bonatto Minella, X. Yu, A. Manthiram, R. J. Behm, M. Ruben, M. Fichtner, *ACS Energy Lett.* **2018**, *3*, 2005.
- [19] Z. Li, X. Mu, Z. Zhao-Karger, T. Diemant, R. J. Behm, C. Kübel, M. Fichtner, *Nat. Commun.* **2018**, *9*, 5115.
- [20] B. O. Jeong, S. W. Kwon, T. J. Kim, E. H. Lee, S. H. Jeong, Y. Jung, *J. Nanosci. Nanotechnol.* **2013**, *13*, 7870.
- [21] T. Yamamoto, H. Etori, *Macromolecules* **1995**, *28*, 3371.
- [22] X. Sun, P. Bonnick, V. Duffort, M. Liu, Z. Rong, K. A. Persson, G. Ceder, L. F. Nazar, *Energy Environ. Sci.* **2016**, *9*, 2273.
- [23] O. Tutusaus, R. Mohtadi, N. Singh, T. S. Arthur, F. Mizuno, *ACS Energy Lett.* **2017**, *2*, 224.
- [24] S. Wang, L. Wang, K. Zhang, Z. Zhu, Z. Tao, J. Chen, *Nano Lett.* **2013**, *13*, 4404.
- [25] J. Bitenc, A. Vizintin, J. Grdadolnik, R. Dominko, *Energy Storage Mater.* **2019**, *21*, 347.
- [26] F. Stenman, *J. Chem. Phys.* **1969**, *51*, 3413.
- [27] H. B. G. Pawelke, *Spectrochim. Acta Part A* **1979**, *35*, 517.
- [28] T. S. Mathis, N. Kurra, X. Wang, D. Pinto, P. Simon, Y. Gogotsi, *Adv. Energy Mater.* **2019**, *9*, 1902007.
- [29] X. Yang, A. L. Rogach, *Adv. Energy Mater.* **2019**, *9*, 1.
- [30] M. D. Levi, E. Lancry, H. Gizbar, Y. Gofer, E. Levi, D. Aurbach, *Electrochim. Acta* **2004**, *49*, 3201.
- [31] M. Mao, X. Ji, S. Hou, T. Gao, F. Wang, L. Chen, X. Fan, J. Chen, J. Ma, C. Wang, *Chem. Mater.* **2019**, *31*, 3183.
- [32] Y. Wang, Z. Liu, C. Wang, Y. Hu, H. Lin, W. Kong, J. Ma, Z. Jin, *Energy Storage Mater.* **2020**, *26*, 494.
- [33] C. N. Gannett, L. Melecio-Zambrano, M. J. Theibault, B. M. Peterson, B. P. Fors, H. D. Abruña, *Mater. Reports Energy* **2021**, *1*, 100008.

Manuscript received: July 13, 2021

Revised manuscript received: August 30, 2021

Accepted manuscript online: September 5, 2021

Version of record online: September 21, 2021